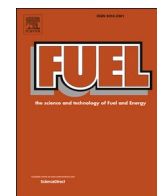# Assessment of experimental methods for measurements of the horizontal flow of fluidized solids under bubbling conditions

(article starts on next page)

Full Length Article

Assessment of experimental methods for measurements of the horizontal flow of fluidized solids under bubbling conditions

Munavara Farha [a,*], Diana Carolina Guío-Pérez [a], Jesper Aronsson [b], Filip Johnsson [a], David Pallarès [a]

[a] *Chalmers University of Technology, Hörsalsvägen 7B, 412 96 Gothenburg, Sweden*
[b] *BioShare AB, Steffens Väg 431, 655 92 Karlstad, Sweden*

ABSTRACT

Dual fluidized bed systems are indispensable for future energy systems that require solids cycling between different atmospheres. However, controlling the residence time of solids in the reactor, which is crucial for controlling the heat and mass transfer of the fuel, is a significant challenge. This study investigates four experimental techniques to quantify the horizontal flow of solids fluidized under bubbling conditions: integral mass accumulation; differential mass accumulation; thermal tracing; and magnetic solids tracing. Integral mass accumulation entails collecting bed material using a defluidized box within a given time period. Differential mass accumulation measures the material accumulation rate in a section of the bed that is monitored using pressure measurements. Thermal tracing calculates the solids flow rate by solving the heat balance to match the temperature field captured by a thermographic camera. Magnetic solids tracing involves injecting a batch of magnetic tracer solids into the reactor and then measuring the residence time distribution using impedance coils.

The experiments were conducted under down-scaled conditions that resemble large-scale operations with a length scaling factor of 0.12. For this study, three operational parameters were varied: the fixed bed height; the volumetric flow rate of the conveying air; and the fluidization velocity in the bed. The horizontal solids circulation rates achieved ranged from 1.7×10^{-4} to 10 kg/m·s, corresponding to 1.2×10^{-3} to 70 kg/m·s on a hot up-scaled basis, which is a relevant range to indirect biomass gasification in an industrial setting.

The three selected operational parameters led to increases in the horizontal solids flow. While all four methods replicated the trends, quantitative variations in the measured circulation rates occurred due to the inherent characteristics of the methods. High circulation rates resulted in a continuous decrease in the solids inventory, leading to an underestimation of the circulation rate when using the integral mass accumulation method. The accuracy of the differential mass accumulation method relied on transient pressure measurements, which were less-effective at low solids flow rates. Conversely, the accumulation time required for pressure measurements was reduced at high circulation rates, resulting in uncertainties in the analysis. The accuracy of the thermal tracing method decreased drastically with higher solids circulation, resulting in an overestimation of the circulation rate. Moreover, low circulation rates adversely affected the accuracy of the magnetic solids tracing by producing barely discernible tracer concentration gradients.

1. Introduction

Since the 1920s, the fluidized bed technology has been applied in numerous industrial applications, including coal and biomass combustion and gasification, fluid catalytic cracking, polymerization, food processing, and chemical synthesis [1].

Dual fluidized bed (DFB) systems consist of two interconnected fluidized beds between which solids circulate. DFB systems are gaining attention because applications that require solids circulation or cycling between different atmospheres are anticipated to play an essential role in the development of the future energy system. These applications include indirect gasification or pyrolysis [2], chemical [3] and calcium [4] looping processes, and thermal and thermochemical energy storage in granular media [5]. The most-extensive operational experience with these energy-related applications has been gained with indirect

---

Nomenclature

A	Cross-sectional area [m^2]
C	Concentration [kg/m^3]
$C_{p,F}$	Specific heat capacity of gas [kJ/kg·K]
$C_{p,S}$	Specific heat capacity of solid particles [kJ/kg·K]
D	Equivalent bed diameter [m]
$D_{S,lat}$	Solids' lateral dispersion coefficient [m^2/s]
d_S	Particle diameter [μm]
$F'*$	Normalized solids circulation rate [kg/m·s]
Fr	Froude number [-]
g	Gravity constant, 9.81 [m/s^2]
G_S	Solids' circulation rate [kg/m^2·s]
Δh	Differential height [m]
H	Bed height [m]
H_b	Expanded bed height [m]
k	Calibration factor of inductance [-]
L	Length [m]
m	Mass [kg]
$\dot{m}$	Mass flowrate [kg/s]
Δp	Differential pressure [Pa]

PSD	Particle size distribution [-]
Re_F	Reynolds number [-]
t	Time [s]
T	Temperature [K]
ΔT	Temperature difference [K]
u_0	Fluidization velocity [m/s]
u_F	Gas velocity [m/s]
u_S	Solids' velocity [m/s]
x	Horizontal position [m]
Z	Background inductance of the coil [H]
Z_0	Measured inductance with the tracer material [H]

Greek letters:

ε_g	Bed voidage [-]
ρ_B	Bulk density [kg/m^3]
ρ_F	Density of gas [kg/m^3]
ρ_S	Density of solid particles [kg/m^3]
μ_F	Gas viscosity [Pa·s]
λ	Effective thermal tracing conductivity [W/m·K]
φ	Particle sphericity [-]

gasification, which entails converting a solid fuel (typically biomass) into combustible gases with high heating value [6].

DFB systems offer flexibility in that each of the fluidized beds combined can be operated under circulating or bubbling conditions, i.e., with or without significant vertical entrainment of solids. The presence in a DFB system of a circulating fluidized bed (CFB) implies the use of vertical entrainment to achieve and control the circulation of solids in the system, which has been exploited in different DFB designs to date. Paisley [7] developed the Battelle biomass gasification process (50 MW$_{el}$), which comprises a steam CFB gasifier interconnected with an air CFB combustor. Rauch et al. [8] demonstrated indirect gasification in a plant in Güssing (8 MW$_{fuel}$) that is based on a steam-fluidized bubbling fluidized bed (BFB) gasifier and generates biogas and an air-fluidized CFB combustor, supplying the heat required for gasification through the circulating bed material. The Twin IHI Gasifier (TIGAR), which combines a CFB combustor and a BFB gasifier, is proficient at producing high-calorific syngas from low-grade coal and biomass fuels (up to a feeding rate of 30 t/day of dry biomass, i.e., roughly 15 MW$_{th}$) [9]. A similarly designed plant was built at Chalmers University of Technology [10] where an existing 8–12-MW$_{th}$ CFB boiler was added to a 2–4-MW$_{th}$ indirect BFB gasification section, with horizontal solids flow observed across the latter section. Pfeifer et al. [11] developed a pilot plant (0.1 MW$_{fuel}$) for hydrogen-rich syngas production from a fast-internally CFB combustor interconnected with a steam BFB gasifier. Developed by ECN [12], the MILENA technology uses a riser for gasification and a BFB for combustion (0.8 MW$_{th}$).

While DFB systems typically contain at least one CFB reactor, which drives the circulation of solids within the system, the BFB/BFB remains a less-intensely investigated configuration despite its potential for increased compactness and operational simplicity, mainly due to the limited experience acquired with the conveyance of solids under bubbling conditions. Matsuoka et al. [13] utilized such an indirect gasification system that was characterized by identical internal diameters (0.08 m) of the gasifier and the combustor, and a height between the gasifier and the top of the cyclone of 1.8 m. Foscolo [14] developed a DFB system for air gasification of low-density biomass that consisted of two interconnected BFBs, producing a low-calorific-value fuel gas (4–5 MJ/Nm^3 dry). Wee et al. [15] developed a syngas production system that consisted of a fluidized bed with two air-blown BFBs – a combustor and a gasifier (i.d. 0.484 m and height 1.8 m).

Establishing appropriate solids circulation remains the main challenge in the design and operation of DFB systems, as these parameters strongly impact the mass and heat balances of each reactor. Therefore, there is interest in investigating means to measure and control the solids circulation in DFB systems. Typically, the magnitudes of the solids circulation rates attained in industrial-scale fluidized bed boilers is are in the range of 5.5–112 kg/m·s, contingent upon the boiler's capacity, which can range from 12 to 235 MW$_{th}$ [16–20]. The determination of solids circulation rate has, consequently, almost exclusively been studied for single-CFB systems, wherein solids circulate through a primary cyclone with inflow from the upper part of the CFB reactor, and after cyclone capture, they flow through a solids return system that feeds them back into the lower part of the CFB reactor. While various measurement techniques have been employed in the literature, they have in common that the solids flow rate is measured in the solids return system. In the study of Karamanev et al. [21], a particle flowrate-measuring device was used, consisting of a butterfly valve positioned between the riser column and a storage vessel, which measured the particle accumulation time via a valve switch mechanism equipped with an indication of pressure change. Matsuda [22] used an optical mouse sensor to measure the descending velocity of the solid particles in the downcomer of the CFB system. A butterfly valve composed of an air plenum and a porous plate was used by Djerf et al. [23] to measure the external solids circulation rate in a CFB cold flow model. Dietrich et al. [24] used alternating activation/deactivation of screw conveyors and loop seals to calculate the circulation rate of solids returning from the cyclone separator into the CFB unit's riser. Kim et al. [25] used an impact probe for measuring the downflow motion of solid particles in a gas-solids suspension; the probe was placed in the downcomer of a CFB system and the measurements were then correlated to the differential pressure. Schiewe et al. [26] used a combination of a laser Doppler anemometer and capacitance probes to measure the velocities of tracer particles in the gas phase and the local solids volume fraction in a downward vertical gas–solid flow. Guío-Pérez et al. [27,28] used the tracking of fluid-dynamically similar ferromagnetic tracer particles to determine the solids circulation rate in a CFB/CFB system [29]; the measurements were based on the impedance change induced in coils located at different positions in the unit. Wang et al. [30] studied the hydrodynamics of a gas–solid system in a CFB riser using an acoustic emissions detection device with a waveguide. Spenik et al. [31] calculated the solids circulation rate in a CFB riser by capturing the particle impingement rate with a piezo-electric pressure transducer probe.

Table 1 compares the solids circulation rates assessed in previous experimental works, utilizing diverse measurement techniques. However, the comparability of such results may be impeded by the differences in various interdependent variables, such as reactor design, operating conditions, measurement principles, and bed material properties, which may influence the outcomes. Within the context of CFB systems, vertical entrainment is most often the mechanism responsible for solids transport. Accordingly, to establish a standardized and consistent basis for a comparative analysis, a normalization process based on the hydraulic diameter of the riser has been incorporated into the values obtained from the selected articles.

Furthermore, computational fluid dynamics (CFD) simulations can serve as a complementary tool for studying the gas-solids flow. In their investigation, Nguyen et al. [37] utilized measurements of particle rising time in a transparent downcomer to evaluate the solids circulation rate and solids holdup in a DFB reactor, while a CFD simulation based on an Eulerian model was employed to solve the governing equations of the system. Hanchate et al. [38] employed experimental data on solids circulation rates in a cold-flow DFB to develop a multiphase Eulerian model. Despite these advances, methods for quantifying the flow rates of conveyed solids under bubbling conditions remain under-developed, and this currently limits the development of DFB applications in the BFB/BFB configuration.

The primary objective of this study is to present and assess the suitability levels of four methods for the experimental determination of solids circulation rates under bubbling conditions. A novel aspect of this study is the development of techniques for measuring solids flow rates in this context, an area that has not been covered in the literature, which instead has focused on measurements in circulating conditions and/or downcomers. Furthermore, it should be emphasized that the scope of this study is restricted to the exploration of the fluidization behaviors of group-B solids under the bubbling regime (fluidization number $\leq$ 4), with solids lateral circulation being constrained to approximately 100 kg/m^2·s on an upscaled basis. The work uses a fluidized bed with a closed loop of horizontal forced solids circulation operated under bubbling conditions. The unit is designed and operated according to scaling laws to simulate the large-scale conditions associated with biomass gasification. The performances of the four experimental methods assessed are evaluated under different conditions by varying the three key operational parameters: bed height; gas flow rate in the solids-conveying zone; and fluidization velocity in the bed.

2. Experimental work

2.1. Fluid-dynamic scaling

Fluid-dynamic downscaling offers the possibility to operate smaller models at room temperature, which means that they resemble the gas-solids flows established in larger geometries under hot conditions. Cold flow models provide increased operational and geometrical flexibilities, reduce restrictions related to implementing diagnostic tools and yield safer and cheaper experimental procedures. The simplified set of scaling laws proposed by Glicksman [39], which was applied to design and operate the scaled-down model used in this work, involves keeping constant the following dimensionless numbers:

$$\frac{u_0^2}{gD}, \frac{\rho_S}{\rho_F}, \frac{u_0}{u_{mf}}, \frac{G_S}{\rho_S u_0}, \frac{L_1}{L_2}, \varphi, \text{PSD}$$

The experimental unit utilized in this study was designed with a length scaling factor of 0.12, which was determined based on the Froude number using Eq.(1). This scaling factor was selected to correspond to the experimental conditions of hot (air/flue gas at 750°–800 °C) and cold (air at 24 °C).

$$[L] = \frac{L_{COLD}}{L_{HOT}} = \frac{\left[\frac{u_{mf}^2}{g \cdot Fr}\right]_{cold}}{\left[\frac{u_{mf}^2}{g \cdot Fr}\right]_{hot}} = \left(\frac{[u_{mf}]_{cold}}{[u_{mf}]_{hot}}\right)^2 = 0.12 \quad (1)$$

The simplified set of scaling laws [39,40] is an experimentally validated tool [23,39,41] that substitutes the Reynolds number with the ratio: u_0/u_{mf}. Thus, while indirectly accounting for the similarity in the fluid-particle interaction, greater flexibility is offered in relation to the choice of length scaling, as this depends on the combination of solids and gas used (as seen from Eq. (1)). Finally, the dimensional analysis yields $[M] = \frac{\rho_{cold}}{\rho_{hot}}[L]^3$ (3.309 in this work, resulting from the solids densities used – see Table 2), considering the conservation of Froude number together with constant gravity yields $[T] = \sqrt{[L]}$ (thus, 0.346 in this work).

Specifically, it should be mentioned that while the solids circulation in CFB units is typically normalized to the cross-sectional area of the riser (thus yielding units kg/m^2·s), the forced lateral circulation of solids within the framework of a BFB is normalized to the width of the solids-conveying region, yielding $F'*$ (in kg/m·s). Using dimensional analysis, the scaling factor for $F'*$ results in:

$$F'* = \frac{F'_{COLD}}{F'_{HOT}} = \frac{[M]}{[L] \cdot [T]} = 0.138 \quad (2)$$

2.2. Experimental setup

The cold flow model (CFM) used (see Fig. 1) operates under bubbling conditions and consists of a closed horizontal loop for the solids, which is created by the presence of a central rectangular solid region ("centre box" in Fig. 1). The unit has a total cross-section of 0.5 m × 0.4 m and a height of 0.5 m. Essentially, this design is intended to house a conveyed lateral flow of fluidized solids under bubbling conditions. A conveying zone (the detailed geometry of which is not relevant for this work) forces a lateral flow of solids, which is conveyed along the loop in a clockwise direction through four so-called 'transport zones' around the center box. The width of transport zone 2 (W_{cold} = 0.052 m) is used to dimension the cold flow model, as it corresponds to the down-scaled value for the width of the connection channel in the design of an industrial DFB system (W_{hot} = 0.43 m). Note that these values are related via the length scaling factor, $[L]$ [Eq. (1)].

All five different zones have their plenum and airflow controllers. In this work, the airflow to the conveying zone is varied independently of that of the transport zones operated with the same fluidization velocity for a given test run. The operation of the CFM involves a hybrid approach of manual control and software-enabled control. While the rotameters are adjusted manually, the mass flowmeters can be regulated and manipulated through the software. Moreover, pressure transducers are utilized to monitor pressure levels in the system, thereby providing valuable information regarding the solids' behaviors within the system.

Flow and temperature fluctuations are inherent to the fluidized bed technology. Measurement accuracy is not affected by these fluctuations, since the calibrations and/or determinations of different parameters measured in this work (pressure, temperature, impedance, etc.) are performed on the basis of time-averaging and/or filtering.

2.3. Test matrix

The test matrix includes variations of the fixed bed height, the fluidization number (FN) in the transport zones, and the airflow provided to the solids-conveying zone. The first two parameters were varied to investigate the sensitivity of the experimental method to the fluidized bed properties (height and voidage). Variation of the airflow provided to the solids-conveying zone was aimed at achieving different solids flow rates. The operational ranges investigated in this work correspond to the operational conditions considered relevant for indirect biomass gasification on an industrial scale. Furthermore, experimental constraints,

Table 1
Comparative analysis of solids circulation rates reported in the literature.

Reference	Configuration		Particle characteristics		Operating conditions		Measurement technique	Solids circulation rate range (kg/m · s)		
Medrano et al. [32]	CFB (concentric, internally circulating)		Glass/Sand/Activated alumina		Medium	Air	Particle extraction	0.078	–	0.48
	H	2.2 m	ρ_S	2,500/2,600/1,135 kg/m³	u_{mf}	0.21 m/s	Particle image velocimetry	0.084	–	0.46
	W_{AR}	0.07 m	d_S	250–500/460/510 μm	u_{FR}	1.2–2.0 u_{mf} m/s	Pressure transducers	0.18	–	0.78
	W_{FR}	0.07 m			u_{AR}	13–24 u_{mf} m/s				
Rahman et al. [33]	DFB		Sand		Medium	Air (Combustion)	Thermal tracing	2.45	–	3.06
	H	6.28 m				Steam (Gasification)	Butterfly valve	1.53	–	2.75
	D	0.08 m			u_{Riser}	6.3–7.3 m/s	Pressure balance	2.45	–	3.37
Dinh et al. [34]	DFBG		Sand		Medium	Air	Mass accumulation	1.98	–	5.74
	H	5 m	ρ_B	1,515 kg/m³	u_{mf}	0.21 m/s				
	D_{CFB}	0.1 m	PSD	149–595 μm	u_{CFB}	21.4–28.6 u_{mf} m/s				
	W_{BFB}	0.18 m			u_{BFB}	1.9–2.6 u_{mf} m/s				
Monazam et al. [35,36]	CFB		Cork		Medium	Air	Rotating spiral vane	0.2	–	5.67
	H	15.3 m	ρ_S	189 kg/m³	u_{mf}	0.17 m/s				
	D	0.3 m	PSD	500–1,500 μm	u_{Riser}	17.7–58.8 u_{mf} m/s				
Guío-Pérez et al. [27–29]	DCFB		Bronze		Medium	Air	Magnetic tracing	0.59	–	5.12
	H	1.56 m	ρ_S	8,730 kg/m³	u_{mf}	0.017 m/s	Mass accumulation	0.79	–	5.70
	D_{FR}	0.054 m	d_S	68 μm	u_{FR}	47.3–106.5 u_{mf} m/s				
	D_{AR}	0.05 m			u_{AR}	82.8–248.5 u_{mf} m/s				
Matsuda [22]	CFB		Sand		Medium	Air	Optical mouse	1.38	–	2.75
	H	4 m	ρ_B	1,239/1,322 kg/m³	u_{Riser}	1.5–3.7 m/s				
	$D_{Dwncomer}$	0.05 m	d_S	191/354 μm						
	D_{Riser}	0.024 m								
Kim et al. [25]	CFB		Sand		Medium	Air	Impact probe	0.39	–	3.14
	H_{Riser}	7.6 m	ρ_S	3,120/2,582 kg/m³	u_{mf}	0.01/0.05 m/s				
	D_{Riser}	0.1 m	d_S	101/240 μm	$u_{Purging}$	3.6–7.2 m/s				
	$H_{Dwncomer}$	4.8 m								
	$D_{Dwncomer}$	0.1 m								
Spenik et al. [31]	CFB		Polyethylene		Medium	Air	Piezo-electric transducer	5.57	–	49.18
	H	15.4 m	ρ_S	864 kg/m³	u_{Riser}	0.47–0.65 m/s	Spiral vane	5.25	–	37.70
	D_{Riser}	0.31 m	d_S	900 μm						

Table 2
Main parameters used in the fluid-dynamically scaled model.

Parameter	Units	Hot unit	Cold model
Temperature	°C	750–800	24
Gas density (ρ_F)	kg/m³	0.359	1.187
Gas viscosity (μ_F)	m²/s	1.4×10^{-4}	1.54×10^{-5}
Bed geometry	m	L_{HOT}	$0.12 \cdot L_{HOT}$
Particle density (ρ_S)	kg/m³	2650	8770
Mean particle diameter (d_S)	μm	950	125
Gas superficial velocity (u_0)	m/s	$u_{0,HOT}$	$\sqrt{0.12}u_{0,HOT}$
Minimum fluidization velocity (u_{mf})	m/s	0.31	0.108
Solids circulation rate (F')	kg/m·s	F'_{HOT}	$0.138 \cdot F'_{HOT}$

such as air supply capacity limits and too-vigorous splashing of solids, yielding solids losses, were also considered while designing the testing matrix.

The FN in the transport zones was limited within a range of 1.8–4, the fixed bed height was varied within the range of 80–100 mm (0.67–0.83 m on a hot up-scaled basis), and the flow rate of air in the conveying zone was restricted to the range of 95–855 l_n/min (0.013–0.119 m³/s on a hot up-scaled basis). By combining the intermediate values of these ranges, 105 cases were examined for each of the four measurement methods. Each setup was repeated three times, resulting in 1,260 tests.

3. Methods for the measurement of solids circulation

This section describes the four measurement methods, their working principles, and how they were implemented in the experimental setup.

3.1. Integral mass accumulation

This approach, schematized in Fig. 2, utilizes enclosures (Boxes 1 and 2) to accumulate the conveyed bed material over a specific time period, from which the average solids flow rate can be calculated. The purpose of Box 1 is primary collection of bed material for the evaluation of the solids flow rate and, thus, it is easily removed from the system. Box 2 (placed beneath Box 1) is intended to collect solids leakages through the gap between Box 1 and the unit walls (thus, it is placed very tightly

against the unit walls and is more-difficult to remove). The box system is positioned in direct connection to the conveying zone. Initially, Box 1 is empty and bed material is prevented from entering it by vertical sliding walls on each of the two ends (interfacing with the convection zone and transport zone 2, respectively; see Fig. 2). After an initial period (30 s) of bed stabilization, the sliding wall in contact with the conveying zone is removed, allowing bed material to be conveyed and accumulated in the box system. Bed material is accumulated until the solids inventory in Box 1 reaches a height level corresponding to 3.5 kg, i.e., the time length of each test, Δt, varies inversely to the solids-conveying rate. At this point, the sliding wall in connection to the conveying zone is set down once again, Box 1 is retrieved, and the accumulated bed material is weighed to determine the solids circulation rate. The bed material that has leaked and accumulated in Box 2 is weighed after each of the repetitions in each experimental case and is thereby accounted for in the calculation of the solids flow rate.

Thus, having collected a certain mass of conveyed solids in Box 1, Δm, the normalized (time-integrated) solids circulation can be calculated as follows:

$$F' = \frac{\dot{m}}{L} = \frac{\Delta m}{\Delta t \cdot L} \qquad (3)$$

Regarding the limitations of this method, it should be noted that this measurement method is non-steady, i.e., a continuous decrease of the inventory of fluidized solids yields variable fluidized bed heights, which in turn affect the conveyed solids flow rate (Section 4.2). Thus, a balance needs to be found between the measurement duration and its impact on the solids flow rate. The shorter the duration of the measurement, the less-robust the statistics of the mass of bed material collected will be. Fig. 3 illustrates this trade-off by plotting experimental curves of the mass of solids collected against the measurement duration (solids accumulation time in Box 2), for different conveying air flow rates. As seen, the curves tend to adapt to a lower gradient (lower solids flow rate) as time elapses. In contrast, longer times typically provide a lower standard deviation of the mass of solids collected (marked by the bars in each marker). It should be noted that a significant proportion (roughly 10%) of the conveyed solids does not end up in either of the collection boxes but leaks through gaps, which introduces some uncertainty into the measurements. Furthermore, the solids circulation rate is to some

(a)   **(b)**
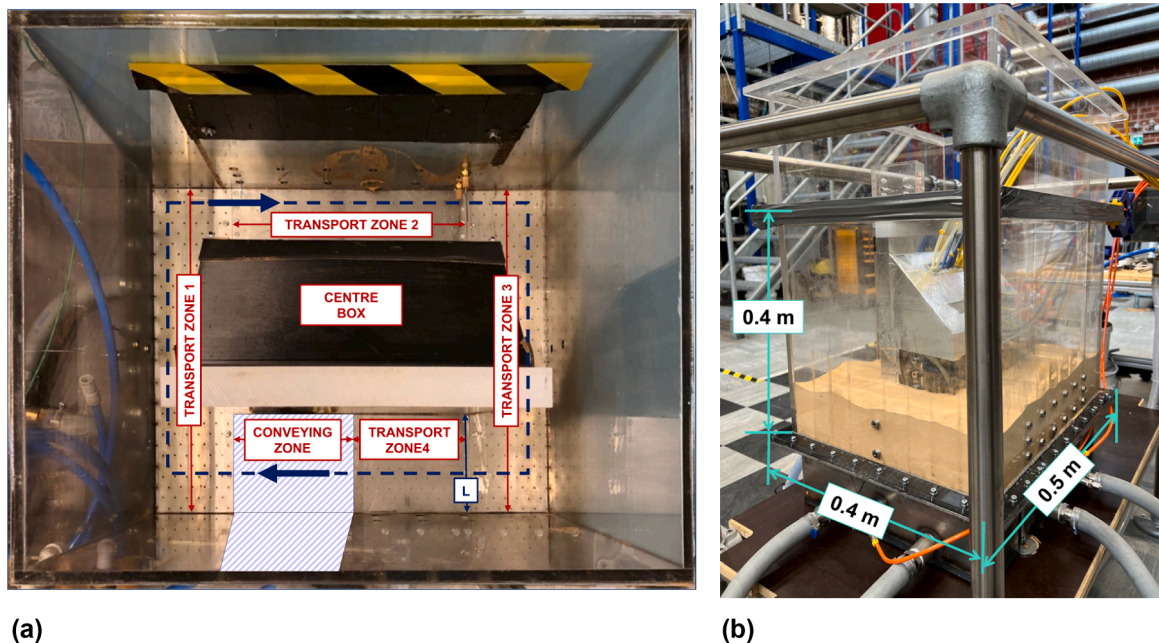
Fig. 1. Fluid-dynamically down-scaled model used for the experiments, where a clockwise solids circulation is forced in the conveying region. (a) Photograph of the top-view, indicating the different regions defined in this work. (b) Photography from the side-view.
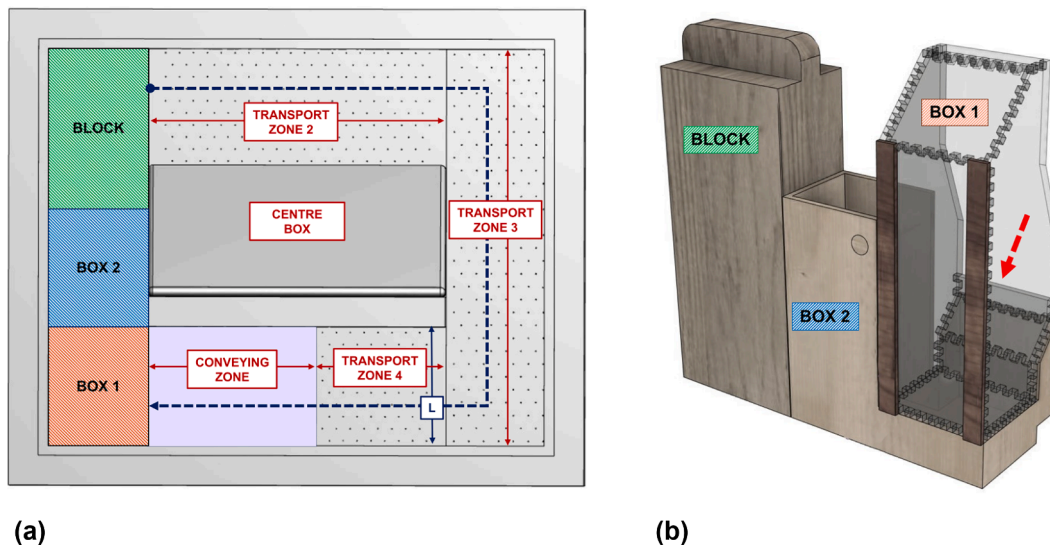
(a)   **(b)**

Fig. 2. Experimental setup used for integral mass accumulation method. (a) Top-view of the unit setting. (b) Box-block arrangement used in transport zone 1.
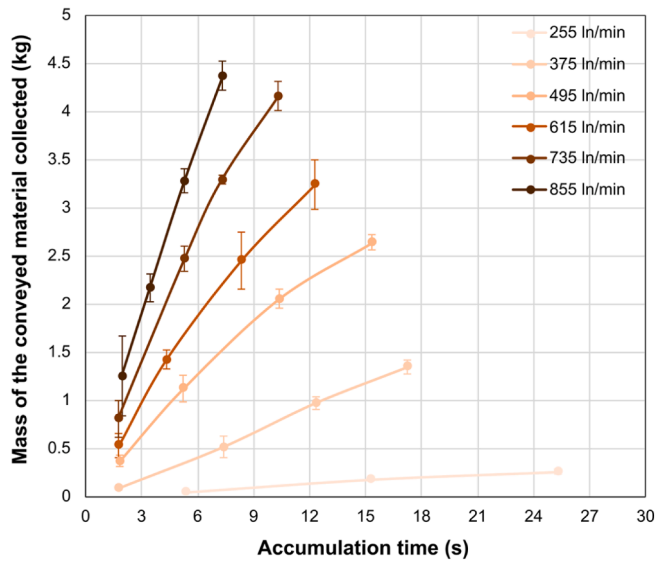

Fig. 3. Impact of collection time on the measurements performed with the integral mass accumulation method. Data for different conveying air flow rates (l_n/min), FN = 2.53 and $H_{b,fixed} = 100$ mm.

extent affected by the length of the circulating loop due to the impact of variable bed-wall friction. Thus, shorter loops caused by the presence of the accumulation box yield lower pressure drops, which means that some overestimation of the solids flow rate is expected. On the other side, it is noteworthy that the solids inventory in the fluidized section decreases as bed material accumulates in the box system; this yields a lower bed and, thus, a constantly decreasing solids flow rate (see Fig. 3).

3.2. Differential mass accumulation

This measurement method employs a sliding wall that can, upon achievement of steady-state conditions with solids circulation, be rapidly inserted vertically along the guide rails positioned at the boundary between transport zones 1 and 2, as depicted in Fig. 4. This insertion establishes an accumulation chamber within transport zone 1 (blue section in Fig. 4a), while the remaining section of the bed (green section in Fig. 4a) empties.

Consequently, the pressure increase in the accumulating zone (and/

or decrease in the emptying zone) can be converted into a solids accumulation rate, i.e., the flow rate of the conveyed solids:

$$F' = \frac{\dot{m}}{L} = \frac{dm}{dt \cdot L} = \frac{dP \cdot A}{dt \cdot g \cdot L} \tag{4}$$

Pressure is sensed at three different levels on both sides of the sliding wall (accumulating and emptying zones): one in the air plenum, and two at distances of 5.25 cm and 7.5 cm from the perforate plate in the bubbling bed. The pressure values measured depend not only on the height but are also observed to vary with the distance to the sliding wall, as a gradient of the bed height is generated within each bed section. However, the distances from the pressure probes to the sliding wall [8 cm, (accumulating zone) and 12 cm (emptying zone), in this setup] (see Fig. 4b) are deemed to be inconsequential in relation to the derived solid flow rates from the signals, as the time derivative is utilized instead of the absolute value.

Fig. 5 exemplifies the pressure transients obtained from the six pressure measurements used in this work. Transient pressure curves tend to flatten out after a certain time (in Fig. 5, this occurs approximately 50 s after the separating wall is slid down), suggesting a maximum capacity for material accumulation, after which a steady state is reached. The accumulating zone has a smaller cross-section and, thus, a more-substantial pressure variation given the same mass flow rate, as compared to the emptying zone. Furthermore, while the accumulating section is fluidized from a single air plenum, thereby ensuring homogeneous fluidization conditions, fluidization of the emptying section involves several air plenums, which entails more-heterogeneous fluidization conditions. Based on this, the transient pressure signals in the accumulating zone are selected for calculating the flow rate of the conveyed solids by taking the average of the time derivatives from the pressure signals at three different height levels. The time interval chosen for the evaluation of the temporal gradient is that for which the variation in the pressure signal deviates from a linear trend (yielding times that are always longer than 10 s).

A primary advantage of this method is its relatively simple implementation. However, the accuracy of the pressure measurements becomes critical, especially at low solids flow rates, since the accumulation is too slow to produce an appreciable change in the pressure. Although minor leakage of materials from the accumulating zone into the emptying zone across the wall-separator gaps are observed at high solids convection rates, it is assumed (based on visual estimation) that this does not significantly impact the results.
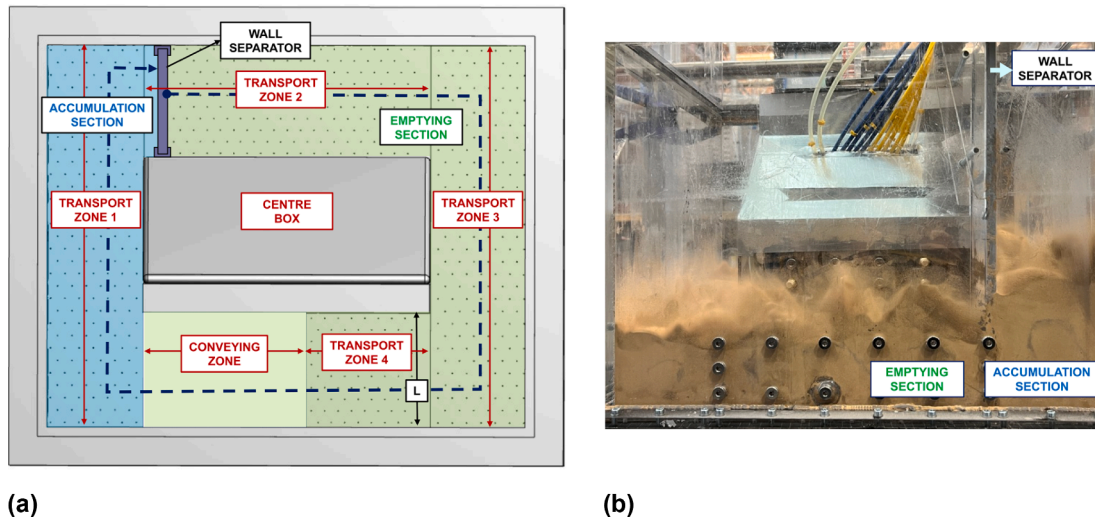
Fig. 4. Experimental setup used for the differential mass accumulation method. (a) Top-view of the unit setting. (b) Wall separator used between transport zones 1 and 2, creating the accumulating and emptying zones.

3.3. Thermal tracing

In this method, as schematized in Fig. 6a, the circulating solids are heated by hot (80 °C) fluidization air as they flow through transport zone 1 ('heating zone'), and they are cooled in the other zones, fluidized with ambient air. The resulting temperature field describing the cooling of the solids flow is used to determine the solids flow rate. This is achieved using the energy equation [42,43], which, if one assumes plug flow pattern for the solid phase and cooling by the fluidization gas, reads as [44]:

$$\left(\rho_S \cdot u_S \cdot (1 - \varepsilon_g) \cdot C_{p,S}\right) \cdot \frac{dT}{dx} = \frac{d}{dx}\left[\lambda \frac{dT}{dx}\right] + \left(\rho_F \cdot u_F \cdot C_{p,F}\right) \cdot \frac{\Delta T}{H_b} \quad (5)$$

where the effective thermal conductivity of the bed, λ, and the solids velocity, u_S are unknowns. Thus, upon determination of the effective thermal conductivity, if the temperature profile along the solids flow direction is determined from measurements, the solids velocity can be solved using Eq. (5). The methodology described by Martinez et al. [44] [see Eqs. (2) and (3) in the reference] entails the use of the effective thermal conductivity for the dispersive transfer of heat, which is governed by the dispersive mixing of the solids ahead of the gas mixing and the static thermal conductivity. Note that the assumption of plug flow for the solids phase is needed to allow consideration of a single value for the solids lateral velocity, u_s. The imprecision of this assumption is considered the main drawback of this method, given that a velocity profile is likely to be established in the transversal direction of the solids flow due to friction between the bed and wall.

Furthermore, the heat balance in Eq. (5) is only representative for the whole bed if the temperature at any location x is representative of the whole bed height. To examine this assumption, a set of thermocouples was installed in the measuring zone, 3 cm and 7.5 cm from the perforated plate, to validate experimentally the uniformity of the vertical temperature profile established within the bed in the measuring zone. The values obtained from the thermocouples were compared to the captured surface temperature profile, and they exhibited very similar values (with a measurement error range of ±0.29 K). In this work, a 1D steady-state, finite volume method is used to solve $T(x)$ in Eq. (5). Note that the measured temperature field is 2D and must be integrated along the y-direction (Fig. 6b), to provide an experimental 1D temperature profile that can be compared with the 1D temperature profile modeled
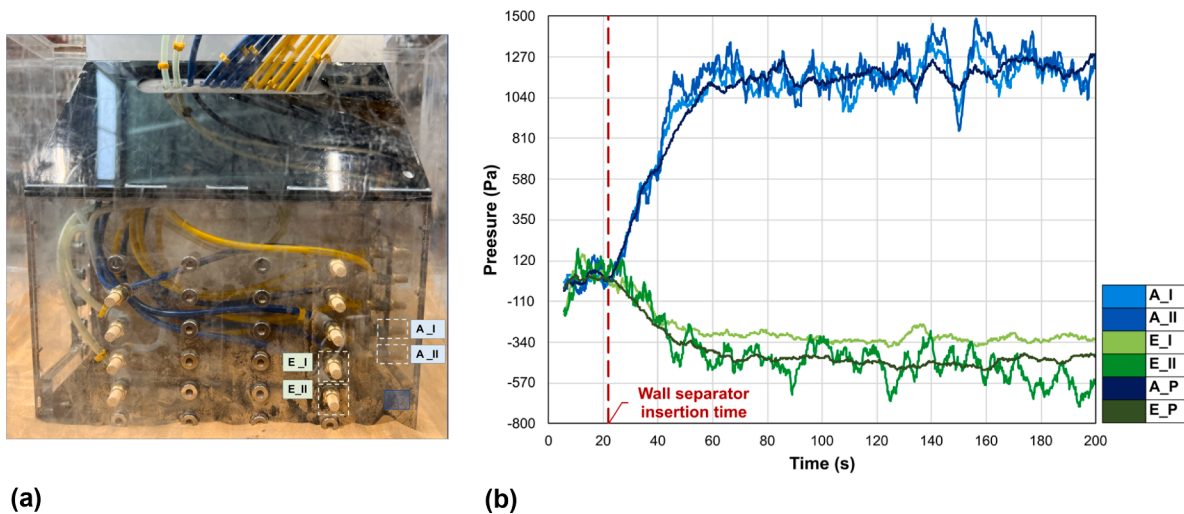
Fig. 5. Differential mass accumulation method. The conditions utilized in the plot were: FN, 3; bed height, 80 mm; and solids-conveying air flow rate, 855 l_n/min. 'A' denotes the accumulation section, 'E' denotes the emptying section, and 'P' denotes the plenum box. (a) Pressure probe locations within the unit. (b) Transient pressure profiles.
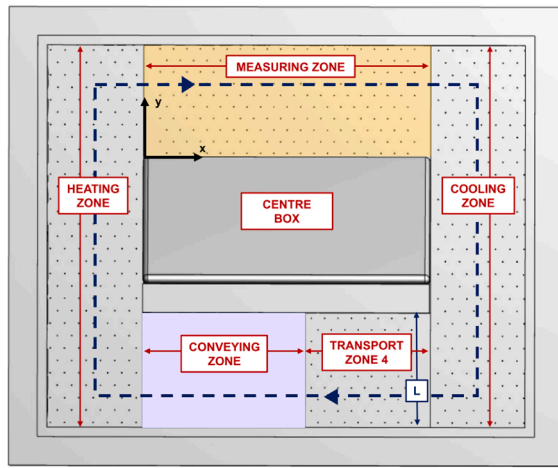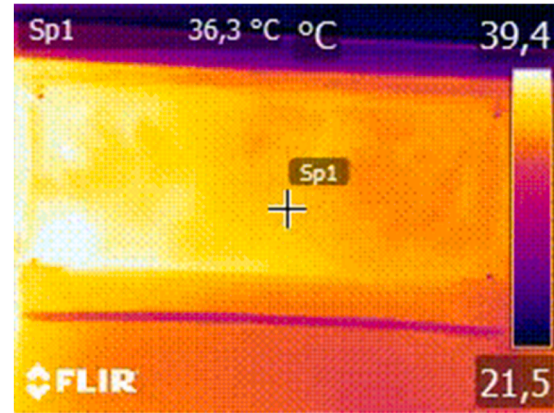
Fig. 6. Experimental setup used for thermal tracing. The temperature scale used is °C. (a) Top-view of the unit setting. (b) Temperature field in the measuring zone captured by the thermographic camera.

using Eq. (5). The Dirichlet boundary conditions are then set using the measured temperature values at the boundaries, T_0 and T_L. One unknown in this equation is the effective thermal conductivity of the bed 'λ', which relates mainly to the solids lateral dispersion coefficient [44], $D_{S,lat}$, according to Eq. (6).

$$D_{S,lat} = \frac{\lambda}{(1 - \varepsilon_g) \cdot C_{p,S} \cdot \rho_S} \tag{6}$$

A thermographic camera (FLIR E53), with a thermal resolution of 240×180 pixels ranging in temperature from -293.15 K to 923.15 K, was used to capture the 2D temperature field over the bed surface in transport zone 2 ('measuring zone'). The camera has a thermal sensitivity of 40 mK. Calibration of the thermographic camera involved adjusting the emissivity factor with the help of simultaneous measurements from the thermocouples. This process is crucial for obtaining accurate temperature measurements, as the camera signal varies under different conditions and includes reflections from the walls, flow fluctuations, etc.

Choosing the appropriate data domain for analysis is crucial in the thermal tracing method. The thermographic profile (240×180 pixels) captured by the infrared camera is analyzed by dividing the field into transversal ($\overrightarrow{y}$) and longitudinal ($\overrightarrow{x}$) slices. Transversal slices exhibit varying results due to the unit's corner geometry, unwanted backflow, and dead zones, which can likely be attributed to the limited length of the measuring zone. Conversely, it is essential to consider wall friction when inspecting the longitudinal slices, as the temperature values close to the wall are significantly lower and yield lower solids flow rates than those acquired at the center of the sampled domain. Therefore, considering all the factors discussed, the analysis domain was selected (Fig. 7a). Integration of the measured 2D temperature field along the *y*-direction yields a 1D experimental temperature representation that can be compared with the temperature profile modeled using Eq. (5).

For each experimental case, the value of the dispersion coefficient, $D_{S,lat}$, is determined in a preliminary experimental run without solids convection. A vertical sliding wall is inserted between the solids-conveying zone and the heating zone, to prevent the macroscopic convection of solids within the system. Thus, in the absence of macroscopic convection, i.e., $u_S=0$ in Eq.(5), λ becomes the only unknown, which allows its determination by fitting the modeled temperature profile to the experimental one. The solids lateral dispersion coefficient in the conveyed flow is assumed to remain the same as that measured under stationary conditions (i.e., in the absence of a net circulation of solids) for the given fluidization velocity and bed height. An example of such a

fitting providing the solids dispersion coefficient is given in Fig. 7b. Having determined the thermal tracing conductivity of the bed, λ [Eq. (6)], the solids velocity, u_S, is determined by fitting the modeled temperature profile given by Eq. (5) to the measured profile with conveyed solids, as exemplified in Fig. 7c. The temperature profile presented in this example corresponds to a high circulation rate. Depending on the solids velocity, a different temperature gradient will be achieved. This fitted value of u_S is then used to determine the normalized solids circulation:

$$F' = \frac{\dot{m}}{L} = u_S \cdot \rho_S \cdot (1 - \varepsilon_g) \cdot H_b \tag{7}$$

The bed voidage, ε_g, [45] is calculated [as in Eq. (8)] for each set of operational conditions utilizing the measurements of the vertical pressure drops sampled inside the bed (6–8 cm from the perforated plate):

$$\varepsilon_g = 1 - \frac{\Delta P}{\rho_S * g * \Delta h} \tag{8}$$

It is important to note that the solids circulation rate is calculated using the expanded bed height, H_b, associated with a given fluidization condition [Eq.(7)].

To mitigate the effects of flow and temperature fluctuations on the thermal measurements, the following approaches have been utilized for this study: system stabilization; appropriate measurement techniques; and employing assumptions. Stabilizing the system necessitates controlling the fluidization velocity in the solids-conveying zone, avoiding changes to the ambient conditions, and ensuring uniform heating or cooling of the system. The accuracy of the thermal tracing method relates to the magnitude of the temperature gradients established in the *x*-direction of the measuring zone. The thermal sensitivity of the thermographic camera (0.04 K) must be compared to the observed temperature difference along the measurement zone, ΔT, which is 0.1 K for the highest solids flow rate (17.88 kg/m·s) and up to 3 K for the lowest solids flow rate (5.07×10^{-3} kg/m·s). Thus, the thermal method becomes less-accurate for high solids flow rates given the limited thermal sensitivity of the temperature measurement. Due to thermal inertia, the wall friction effects, unit geometry, and the degree of inaccuracy increase as the solids circulation rate increases. High fluidization velocities have the potential to introduce uncertainties into the temperature measurements, which are attributed to bubble eruption that subsequently alters the surface temperature and emissivity of the fluidized bed particles.
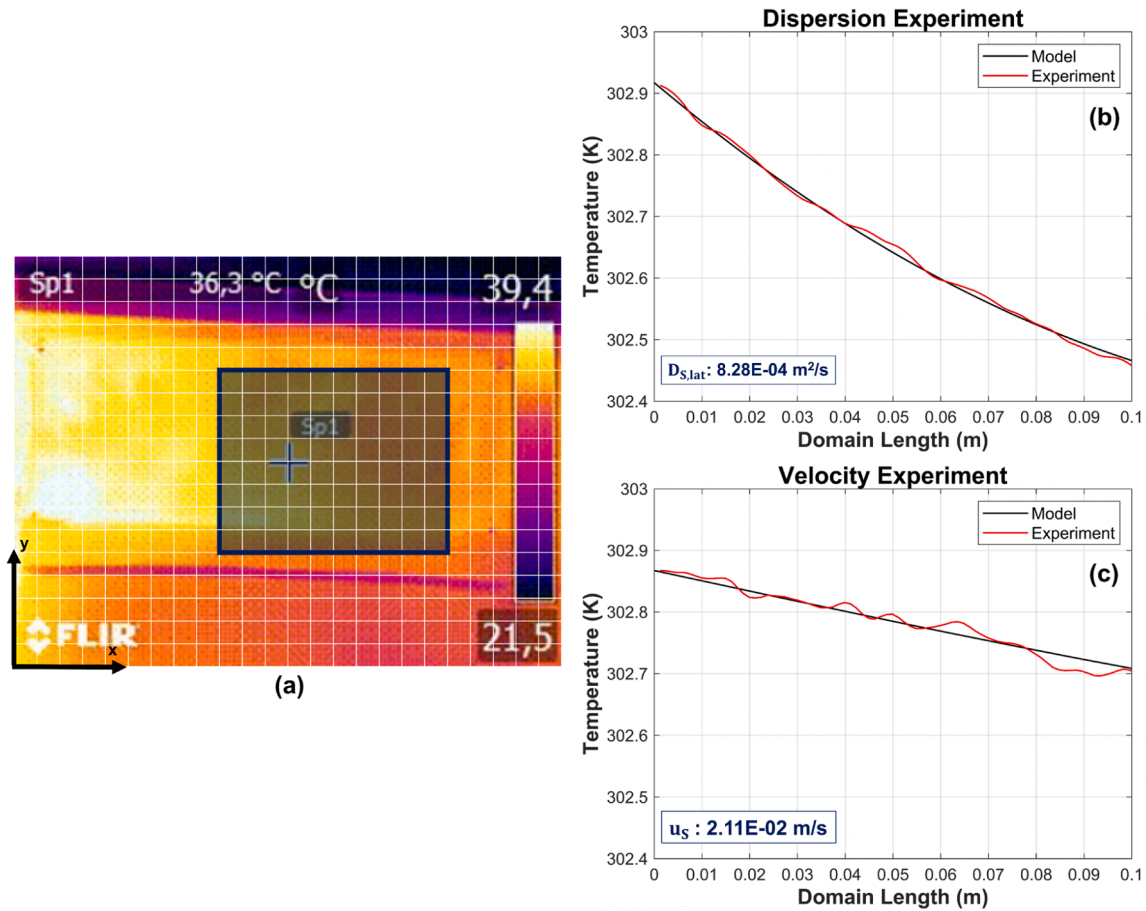
Fig. 7. Thermal tracing method. (a) Sampled temperature field, and longitudinal experimental and modeled temperature profiles in the absence/presence (b/c) of macroscopic solids convection. Experimental conditions set at: FN, 3; bed height, 80 mm; and flow rate of conveying air, 855 l$_n$/min. The temperature scale used is in °C.

3.4. Magnetic solids tracing

A small batch (200 g) of tracer material mimicking the physical properties of the bulk solids (see Table 3) is introduced 14 cm upstream of coil 1. The injection is made by means of a special probe, designed to inject tracer material along the bed height. This is intended to yield an axially mixed injection pulse of bed material that is well-mixed in the vertical direction. The transient concentration of the tracer at different locations is monitored using impedance coils, from which the rate of solids conveyance can be derived. The setup in this work (Fig. 8) uses four rectangular coils, each framing the entire cross-section passed by the solids flow at different locations along transport zone 2 ('measuring zone'). The detection method is based on changes in impedance induced in the coil due to the high permeability of the magnetic tracer solids (details of the detection method can be found in [28]). Since the tracer concentration is sampled over time (100 Hz), the residence time distribution of the tracer material between the different coil locations can be calculated, and from there, the corresponding solids circulation rate can be derived.

A check for signal uniformity within the coil cross-section was performed prior to the experiments. The tracer concentration, C, is calculated from the impedance signal, Z, based on Eq. (9):

$$C = k \cdot \frac{(Z - Z_0)}{Z_0} \qquad (9)$$

where k is the calibration factor of inductance, which depends on the relative permeability of the tracer material used and on the extent to

Table 3
Comparison of the materials used in the bed and magnetic tracer.

Parameter	Unit	Bed		Tracer	
Material	–	Bronze		FeSi 68 HQ	
Particle density (ρ_S)	kg/m^3	7,988.3		8,770	
Bulk density (ρ_{Bulk})	kg/m^3	5,522.1		4,520	
Particle size distribution					
d$_{90}$	μm	79.83		24.78	
d$_{50}$	μm	112.06		68.69	
d$_{10}$	μm	132.45		122.83	
Mean particle diameter (d_S)	μm	125		93	
Chemical composition, %	–	Cu	90	Fe	>25
		Sn	10	SiO$_2$	>1
				Ni	0.1–0.99
				Co	0.1–0.25

which the mixture of bed material and tracer fills the geometry of the coil. This parameter was determined through a separate set of calibration experiments performed for the FNs applied to the transport zones. The data sampling occurs sequentially along the different coils on a one-at-a-time basis, to avoid signal cross-interference..

Table 3 summarizes the comparison of the bed material and magnetic tracer used in the experiments.

Since the experimental configuration used for this method allows solids circulation, the tracer injected at a specific location will be conveyed through the coils several times. The first coil passage will yield a sharp increase in the signal (often in the form of a peak). The increased signal will decline with increasing number of passages until the tracer
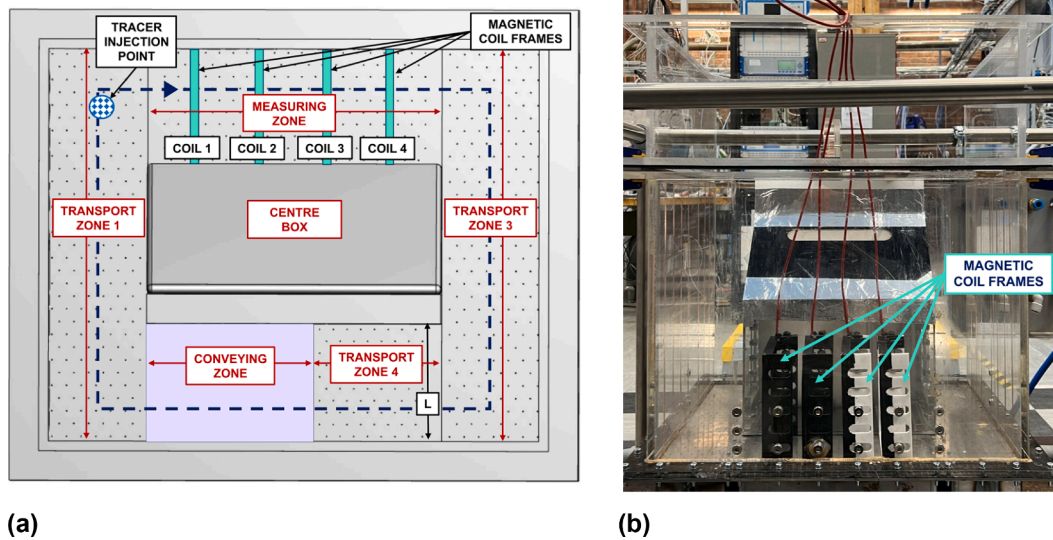
Fig. 8. Experimental setup used for the magnetic solids tracing method. (a) Top-view of the unit setting. (b) Magnetic coil frames placed in the measuring zone.
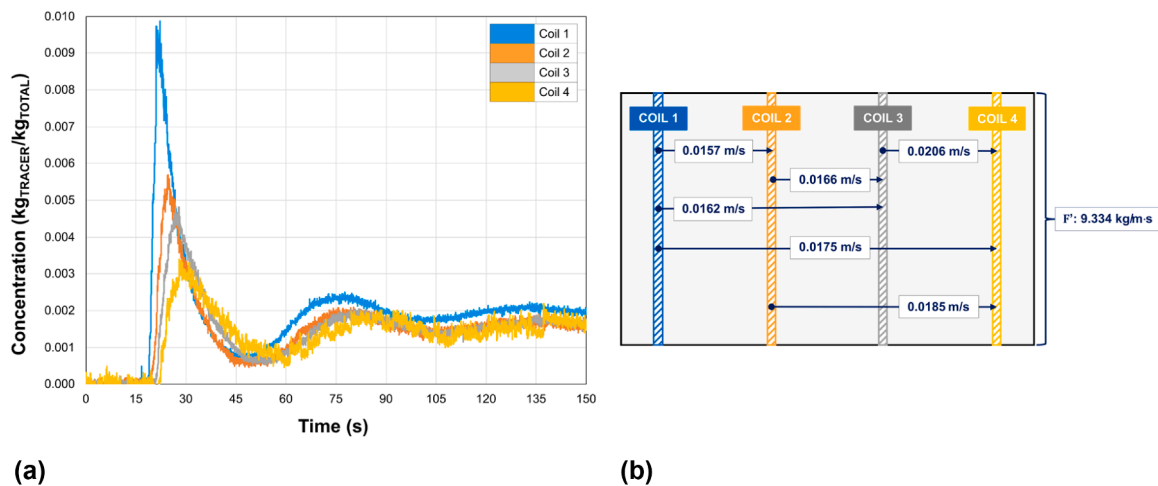

Fig. 9. Example of an analysis based on the magnetic solids tracing technique. Experimental conditions are set at: FN, 1.83; bed height, 100 mm; and volumetric flow rate in the conveying zone, 855 l_n/min. (a) Transient concentration profile. (b) Derived solids velocity values.

concentration is distributed evenly across the bed in a steady-state condition, producing a constant signal from the coils. Afterwards, the tracer material is removed from the bed using a permanent magnet, to conduct the next experiment.

An average solids velocity, u_S, is calculated based on the time delay of the tracer concentration peaks (exemplified in Fig. 9a) observed from the four coils and the distances between them. As displayed in Fig. 9b, the variations in velocity values obtained at different positions of the four coils placed in the measuring zone for the same run are generally consistent ($\sigma \approx 0.0018$ m/s). From this solids velocity, the normalized solids circulation can be calculated using Eq. (7). In this case, similar to the thermal tracing method, it is imperative to consider the value of the bed voidage, ε_g.

The main limitations of this method are the time-consuming separation of the magnetic tracer from the bed material and the limited choice of available tracer materials with physical properties comparable to the bed material. For the specific case of the results presented here, the accumulation of tracer material at the corners of the unit, i.e., tracer segregation, was observed to some extent. Furthermore, low rates of solids circulation produce coil signals with less-distinct gradients of tracer concentration, reducing the method's accuracy.

4. Results and discussion

4.1. Bed voidage

The value for the bed voidage is required in both the thermal tracing and magnetic solids tracing methods. The bed voidage for each FN applied to the transport zones is calculated from the pressure differences between two probes located at different heights inside the bed. The probes (located at 7–8 cm) are above the perforated plate, to avoid disturbance of the pressure measurements by acceleration effects. Fig. 10 shows the increase in bed voidage with FN due to the increased frequency and size of the bubbles [45]. Thus, for the operational conditions considered in this study, the bed height increases with fluidization velocity.

4.2. Solids circulation rate

Fig. 11 compares the solids circulation rates calculated with the four methods. The error bars indicate the range of values obtained for each experimental condition over the repetitions. That these bars, in most cases, are very small indicates the statistical robustness of the data. In general, all four methods capture the same qualitative trends regarding
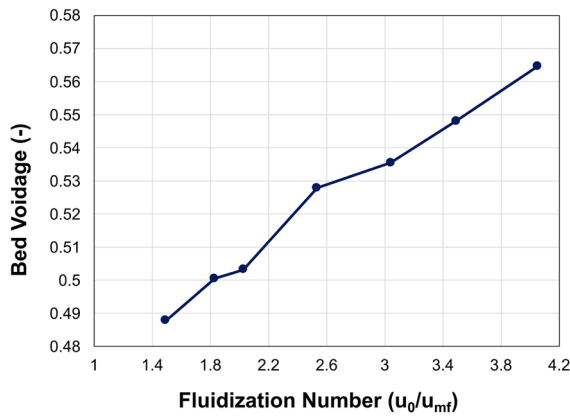
Fig. 10. Measured bed voidage as a function of the fluidization number.

how the three operational variables affect the solids flow rate (an increase in any of the variables yields an increase in the solids flow rate).

The plots in Fig. 11 demonstrate that the two mass accumulation methods – integral and differential – produce similar values of the solid flow rate, with the latter being slightly higher. For both methods, leakages of bed material from the confining volumes result in an underestimation of the calculated solids flow rate, due to the decreased bed inventory. Both methods lack accuracy in relation to measuring low rates of solids conveyance. The integral method fails to reflect differences in circulation rates at low solids-conveying rates. In contrast, the differential method displays variations in pressure signals with an amplitude comparable to ambient noise. However, this can be reduced if the accumulation interval is sufficiently long.

The thermal tracing method consistently yields significantly higher solids circulation rates than the other methods, exceeding by factors of 2.8, 2.5, and 1.4 those provided by the integral mass accumulation, differential mass accumulation, and magnetic solids tracing methods, respectively. The potential overestimation of the solids flow rate by the thermal tracing method is, to some extent, due to the selection of the analysis region. Choosing a central location within the measured domain eliminates wall effects and, thereby, gives a better fit with the modeled temperature profiles. The central location also provides higher solids flux rates than areas closer to the walls. Furthermore, Fig. 11 indicates that the thermal tracing method shows inaccuracies at high levels of solids conveyance, due to the lower temperature gradients established in situations of increased thermal inertia.

The magnetic solids tracing method typically yields solids flow rate values intermediate to those yielded by the thermal and mass accumulation methods. The lateral solids dispersion is expected to add some level of inaccuracy (by diluting the peak in solids concentration), as well as some degree of overestimation (by displacing in time the peak in the coil-measured signal). This effect is enhanced for situations with low solids-conveying rates and conditions in which dispersion can be expected to be high, such as a high fluidization velocity in the transport zones and/or a high bed height. However, given the good stability of the signal, the magnetic solids tracing method is assumed to be the most robust and accurate method in general terms.

It is essential to highlight that the present study aims to evaluate measurement methods and indicate how they can help provide a general understanding of the parameters that influence the horizontal solids circulation rate in coupled beds. Consequently, optimization of the
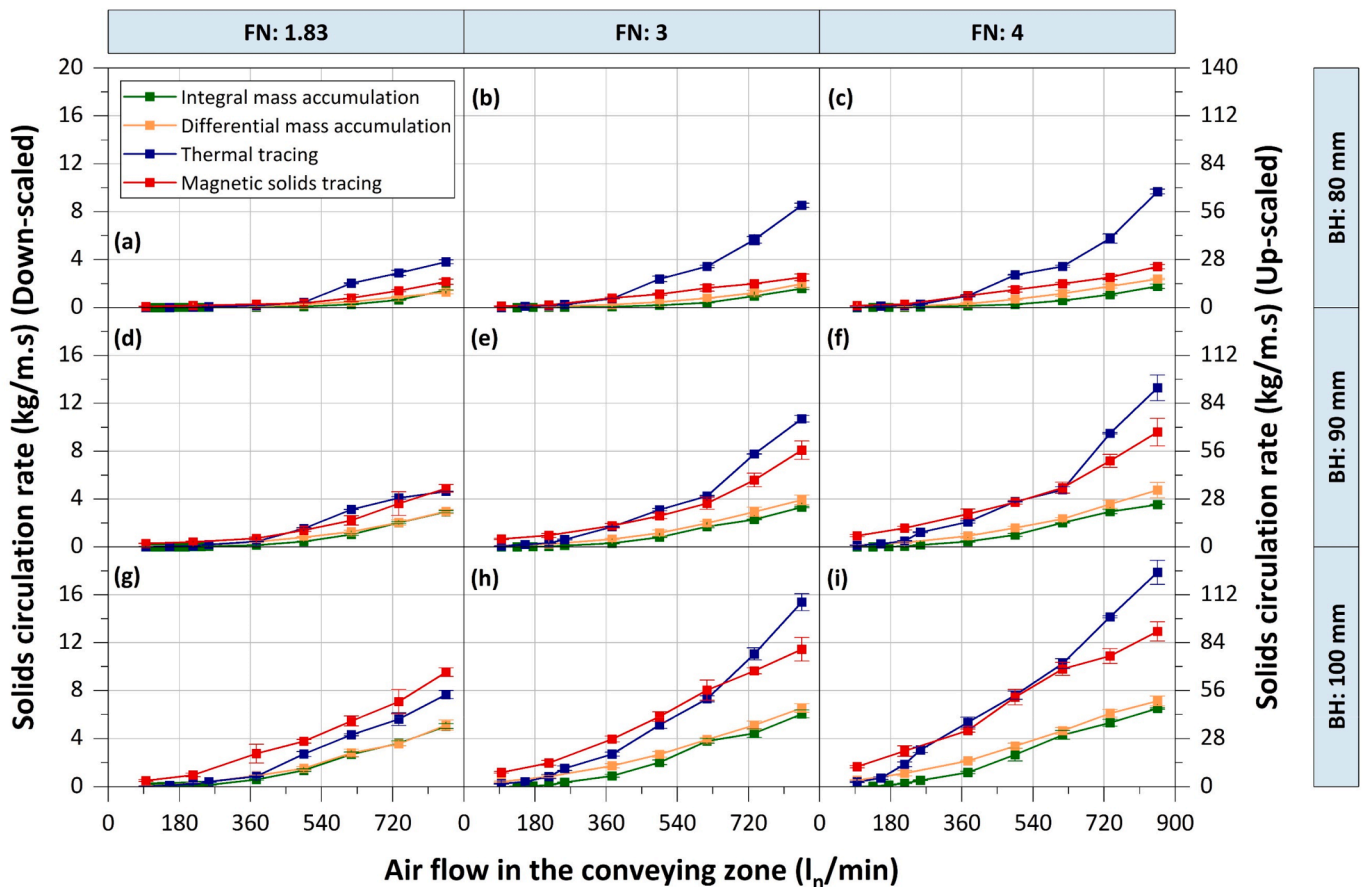

Fig. 11. Normalised solids flow rates measured using the four different methods assessed under different operational conditions. FN, fluidization number in the transport zones; BH, fixed bed height. The bars at each marker indicate the standard deviation of the repetitions.

Table 4
Standardized effect sizes of the parameters obtained for the four methods evaluated.

Method	Standardized effect size		
	Bed height (mm)	Fluidization number in the transport zones (-)	Volumetric flowrate in the solids-conveying zone (l_n/min)
Integral mass accumulation	40.66	9.80	64.00
Differential mass accumulation	36.07	14.37	52.38
Thermal tracing	21.90	21.82	56.60
Magnetic solids tracing	36.42	19.93	48.88

solids-conveying mechanism has not been addressed. The results for solids flow rates obtained in this study can be refined, further mitigating the limitations associated with using specific techniques. With this understanding of the pros and cons of the methodologies used, a regression analysis was conducted to determine how the impacts of the operational parameters on the measured solids flow rates varied across the four methods. The experimentally obtained values in this study range up to 10 kg/m·s, while the previous literature with on solids circulation forced by vertical entrainment (see Table 1) exhibit a spectrum of 7.8×10^{-2}–4.9×10^{1} kg/m·s.

Table 4 reports the standardized effect (SE) size statistics, which is a measure used to evaluate how big or small an effect is when the units of measurement are not intuitive, so they can help compare results across studies (i.e., measurements in this case). The SE measures the statistical significance and magnitude of the measurement data from each method, examined for the three parameters used in the regression modeling (see [46] for details In factorial design, the SE size (also known as Cohen's *d*, please find calculation details in [46]) for each of the parameters used in a correlation is used to determine the relative influences of different factors on the response variable. The analysis of these data can yield valuable insights for designing future experiments and for informed decision-making.

Consequently, an analysis of the direction of the effects is conducted by constructing the main effects plot, as shown in Fig. 12, to determine the relative impacts of the three input parameters on the solids circulation rate. Although the trends are the same (as discussed previously), the statistical analysis indicates differences with respect to their impacts.

Compared to the other two methods, the integral and differential mass accumulation methods exhibit reduced effects of the three operational parameters, due to increased bed material leakage at higher solids flow rates. For these mass accumulations methods, the air flow rate in the solids-conveying zone has the strongest impact on the solids circulation rate (SE of 64 vs. 52), followed by the fixed bed height (SE of ~ 37.5), and the FN in the transport zones (SE of ~ 12). For the thermal tracing method, the magnitude of the effect of the fluidization flow rate in the solids-conveying zone on the solids circulation rate is the highest

(SE of ~ 57). At the same time, the fixed bed height and FN in the transport zones show similar impacts (SE of ~ 22). As this method captures the surface temperature profile, which incorporates splashing and wall effects together with the acquired solids circulation rate, the general trend seen using this method is comparatively amplified. A similar pattern is observed using the magnetic solids tracing method, although it is slightly less-pronounced. This method is affected significantly by the flow rate in the solids-conveying zone (SE of ~ 49), followed by the fixed bed height (SE of ~ 36), and the FN in the transport zone (SE of ~ 20).

The present study is limited in that the assessment regards measurement techniques applied to a cold laboratory-scale (albeit fluid-dynamically down-scaled) unit. Implementation under industrial conditions will present additional challenges for each of the methods assessed here, and alternative – but less accurate – methods, such as macroscopic heat balance, may eventually become better options for monitoring the solids flow.

5. Conclusions

A cold flow model, which was designed and operated according to Glicksman's simplified set of scaling laws, was used to assess four experimental methods for measuring the horizontal circulation of solids under bubbling conditions. Based on the results of this study, the magnetic solids tracing method is recommended as the most-suitable method for measuring horizontal solids circulation under bubbling conditions, due to its robust signal measurement capabilities. However, caution must be exercised when measuring low solids circulation rates, as the tracer concentration gradients may be difficult to discern. The thermal tracing method consistently provides higher solids circulation rates, although is it not accurate due to cropping of the analysis domain to a region that fits the theoretical assumptions, thereby ignoring flow limitations that are coupled to wall friction effects and unit geometry. The integral and differential mass accumulation methods yield lower solids circulation rates than the other methods, especially for conditions with high rates of solid conveyance, due to bed material leakages, a reduction
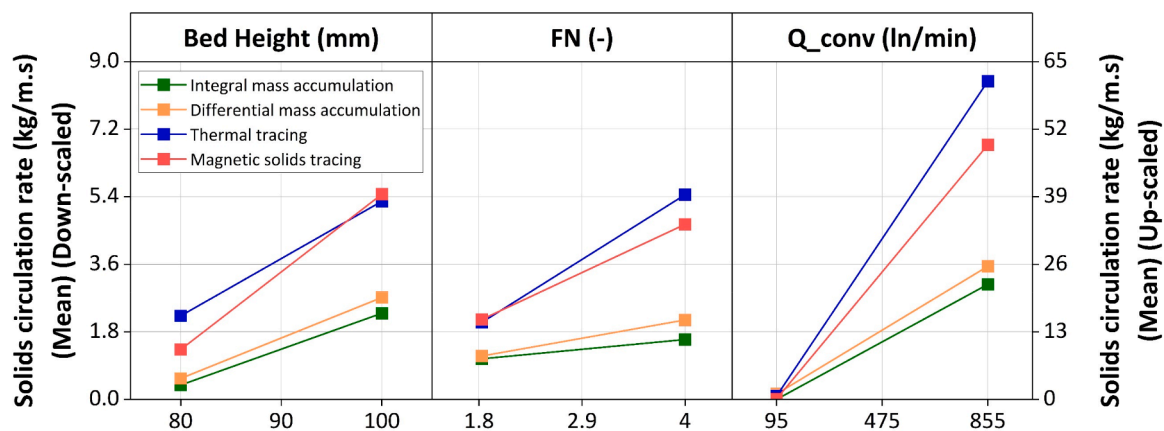
Fig. 12. Plots of the main effects of bed height, fluidization number, and airflow in the conveying zone (Q_{conv}) on the solids circulation rate, for the four methods assessed.

of the measurement time suitable for analysis, and the inevitable reduction of the inventory during performance of the measurements.

Furthermore, it is essential to note that the solids circulation rate increases when the following three operational parameters are varied: the air flow used for conveying the solids; bed height; and fluidization velocity in the bed (in order of their impacts on the rate of solids circulation established).

Future investigations should include evaluations of different configurations and mechanisms for conveying solids in systems under bubbling conditions, as well as explorations of the solids hydrodynamics (study of the bed-wall friction) and mixing characteristics (analyses of the combined convection–dispersion mechanisms).

CRediT authorship contribution statement

Munavara Farha: Investigation, Formal analysis, Validation, Writing – original draft. **Diana Carolina Guío-Pérez:** Conceptualization, Methodology, Supervision, Writing – review & editing. **Jesper Aronsson:** Conceptualization, Resources. **Filip Johnsson:** Writing – review & editing. **David Pallarès:** Conceptualization, Funding acquisition, Supervision, Writing – review & editing.

Declaration of Competing Interest

The authors declare the following financial interests/personal relationships which may be considered as potential competing interests: Munavara Farha reports financial support was provided by Swedish Energy Agency. Munavara Farha reports administrative support and equipment, drugs, or supplies were provided by Bioshare.

Data availability

Data will be made available on request.

Acknowledgements

References

[1] Grace J, Bi X, Ellis N, editors. Essentials of Fluidization Technology. Wiley; 2020.

[2] Pletka R, Brown RC, Smeenk J. Indirectly heated biomass gasiÿcation using a latent heat ballast-1: experimental evaluations; 2001.

[3] Fan L-S, Li F. Chemical looping technology and its fossil energy conversion applications. Ind Eng Chem Res Nov. 2010;49(21):10200–11. https://doi.org/10.1021/ie1005542.

[4] Chang MH, et al. Design and experimental investigation of calcium looping process for 3-kWth and 1.9-MWth facilities. Chem Eng Technol Sep. 2013;36(9):1525–32. https://doi.org/10.1002/ceat.201300081.

[5] Ratuszny P, Wzorek M, Królczyk G, Król A. Thermal energy storage in granular deposits. E3S Web of Conferences EDP Sciences 2017;19:01022.

[6] Guan H, Fan X, Zhao B, Yang L, Sun R. Application and discussion of dual fluidized bed reactor in biomass energy utilization. IOP Conf Ser: Earth Environ Sci Jan. 2018;108(5):052019. https://doi.org/10.1088/1755-1315/108/5/052019.

[7] Paisley MA. In: developments in thermochemical biomass conversion. Dordrecht: Springer Netherlands; 1997. p. 1209–23.

[8] Rauch R, Hofbauer H, Bosch K, Siefert I. Steam gasification of biomass at CHP plant in Güssing - Status of the demonstration plant. In: 2nd World Conference and Technology Exhibition on Biomass for Energy, Industry and Climate Protection, pp. 1687–1690, Jan. 2004.

[9] Toshiyuki S. Gasification of Lignite Coal and Biomass Using Twin IHI Gasifier (TIGAR ®); 2012.

[10] Thunman H, Seemann MC. In: proceedings of the 20th international conference on fluidized bed combustion. Berlin, Heidelberg: Springer Berlin Heidelberg; 2010. p. 659–63.

[11] Pfeifer C, Pröll T, Puchner B, Hofbauer H. H2-rich syngas from renewable sources by dual fluidized bed steam gasification of solid biomass. Fluidization XII, Jan. 2007.

[12] van der Meijden CM, VeringaHJ, van der Drift A, Vreugdenhil BJ. The 800 kWth allothermal biomass gasifier MILENA; 2008.

[13] Matsuoka K, Kuramoto K, Murakami T, Suzuki Y. Steam gasification of woody biomass in a circulating dual bubbling fluidized bed system. Energy Fuel May 2008;22(3):1980–5. https://doi.org/10.1021/ef700726s.

[14] Foscolo PU, Germanà A, Jand N, Rapagnà S. Design and cold model testing of a biomass gasifier consisting of two interconnected fluidized beds. Powder Technol 2007;173(3):179–88. https://doi.org/10.1016/j.powtec.2007.01.008.

[15] Wee SK, Chok VS, Srinivasakannan C, Chua HB, Yan HM. Fluidization quality study in a compartmented fluidized bed gasifier (CFBG). Energy Fuel 2008;22(1):61–6.

[16] Johansson AS. Solids flow pattern in circulating fluidized-bed boilers; 2005.

[17] Yang H, Yue G, Xiao X, Lu J, Liu Q. 1D modeling on the material balance in CFB boiler. Chem Eng Sci Oct. 2005;60(20):5603–11. https://doi.org/10.1016/j.ces.2005.04.081.

[18] Zhang N, Lu B, Wang W, Li J. 3D CFD simulation of hydrodynamics of a 150MWe circulating fluidized bed boiler. Chem Eng J Aug. 2010;162(2):821–8. https://doi.org/10.1016/j.cej.2010.06.033.

[19] Zhang Y, Lei F, Xiao Y. Influence of solids circulation flux on coal gasification process in a pressurized high-density circulating fluidized bed. J Therm Sci Feb. 2019;28(1):97–105. https://doi.org/10.1007/s11630-018-1059-3.

[20] Pandey KM, Ray M. Experimental studies on hydrodynamics of a cyclone separator employed in a circulating fluidized bed. Int J Chem Eng Applications 2010:123–31.

[21] Zhu JX, Zheng Y, Karamanev DG, Bassi AS. (Gas-)liquid-solid circulating fluidized beds and their potential applications to bioreactor engineering. Can J Chem Eng Feb. 2000;78(1):82–94. https://doi.org/10.1002/CJCE.5450780113.

[22] Matsuda S. Measurement of solid circulation rate in a circulating fluidized bed. Powder Technol Oct. 2008;187(2):200–4. https://doi.org/10.1016/J.POWTEC.2008.02.004.

[23] Djerf T, Pallarès D, Johnsson F. Solids flow patterns in large-scale circulating fluidised bed boilers: experimental evaluation under fluid-dynamically down-scaled conditions. Chem Eng Sci 2021;231:116309.

[24] Dietrich F, Tondl G, Wöss D, Pröll T, Hofbauer H. Comparison of four different methods for measuring the solids circulation rate in circulating fluidized beds; 2013.

[25] Kim SW, Ahn JY, Lee DH, Kim SD. Continuous measurement of solids flow in a circulating fluidized bed. Korean J Chem Eng 2001;18(4):555–60. https://doi.org/10.1007/BF02698305.

[26] Schiewe T, Wirth KE, Molerus O, Tuzla K, Sharma AK, Chen JC. Measurements of solid concentration in a downward vertical gas-solid flow. AIChE J 1999;45(5): 949–55. https://doi.org/10.1002/aic.690450505.

[27] Guío-Pérez DC, Dietrich F, Ferreira Cala JN, Pröll T, Hofbauer H. Estimation of solids circulation rate through magnetic tracer tests. Powder Technol 2017;316: 650–7. https://doi.org/10.1016/j.powtec.2017.04.062.

[28] Guío-Pérez DC, Pröll T, Hofbauer H. Measurement of ferromagnetic particle concentration for characterization of fluidized bed fluid-dynamics. Powder Technol May 2013;239:147–54. https://doi.org/10.1016/j.powtec.2013.01.040.

[29] Pröll T, Rupanovits K, Kolbitsch P, Bolhàr-Nordenkampf J, Hofbauer H. Cold flow model study on a dual circulating fluidized bed system for chemical looping processes. Chem Eng Technol 2009;32(3):418–24. https://doi.org/10.1002/ceat.200800521.

[30] Wang J, Ren C, Yang Y, Hou L. Characterization of particle fluidization pattern in a gas solid fluidized bed based on acoustic emission (AE) measurement. Ind Eng Chem Res 2009;48:8508–14.

[31] Spenik JL, Ludlow JC. Use of piezoelectric pressure transducers to determine local solids mass flux in the riser of a cold flow circulating fluidized bed. Powder Technol Oct. 2010;203(1):86–90. https://doi.org/10.1016/J.POWTEC.2010.03.031.

[32] Medrano JA, Nordio M, Manzolini G, van Sint Annaland M, Gallucci F. On the measurement of solids circulation rates in interconnected fluidized beds: comparison of different experimental techniques. Powder Technol Nov. 2016;302: 81–9. https://doi.org/10.1016/j.powtec.2016.08.035.

[33] Rahman MH, Bi XT, Grace JR, Lim CJ. Comparison of techniques for measuring CFB solids circulation rates at low and high temperatures. Powder Technol Jan. 2020;360:43–54. https://doi.org/10.1016/j.powtec.2019.10.033.

[34] Dinh C-B, Hsiau S-S, Su C-Y, Tsai M-Y, Chen Y-S, Nguyen H-B, et al. Full-loop study of a dual fluidized bed cold flow system: hydrodynamic simulation and validation. Adv Powder Technol 2021;32(3):670–82.

[35] Monazam ER, Breault RW, Freed AD, Shadle L, Lawson LO, Rowan SL. Development and validation of a dynamic response model for a cold flow circulating fluidized bed. Ind Eng Chem Res Jan. 2017;56(1):288–300. https://doi.org/10.1021/acs.iecr.6b03536.

[36] Ludlow JC, Monazam ER, Shadle LJ. Improvement of continuous solid circulation rate measurement in a cold flow circulating fluidized bed. Powder Technol Mar. 2008;182(3):379–87. https://doi.org/10.1016/j.powtec.2007.06.031.

[37] Nguyen TDB, Seo MW, Il Lim Y, Song BH, Kim SD. CFD simulation with experiments in a dual circulating fluidized bed gasifier. Comput Chem Eng Jan. 2012;36(1):48–56. https://doi.org/10.1016/j.compchemeng.2011.07.005.

[38] Hanchate N, Korpale VS, Mathpati CS, Deshmukh SP, Dalvi VH. Computational fluid dynamics of dual fluidized bed gasifiers for syngas production: cold flow studies. J Taiwan Inst Chem Eng Dec. 2020;117:156–63. https://doi.org/10.1016/j.jtice.2020.12.014.

[39] Glicksman LR, Hyre M, Woloshun K. Simplified scaling relationships for fluidized beds. Powder Technol 1993;77(2):177–99.

[40] Glicksman LR. Scaling relationships for fluidized beds. Chem Eng Sci Jan. 1988;43 (6):1419–21. https://doi.org/10.1016/0009-2509(88)85118-2.

[41] Mirek P. Influence of the model scale on hydrodynamic scaling in CFB boilers. Braz J Chem Eng Oct. 2016;33(4):885–96. https://doi.org/10.1590/0104-6632.20160334s20150348.

[42] Versteeg HK, Malalasekera W. An introduction to computational fluid dynamics Second Edition. 2007. Accessed: Sep. 08, 2022. [Online]. Available: www.pearsoned.co.uk/versteeg.

[43] Patankar SV. Numerical heat transfer and fluid flow. CRC Press 1980. https://doi.org/10.1201/9781482234213.

[44] Martinez Castilla G, Larsson A, Lundberg L, Johnsson F, Pallarès D. A novel experimental method for determining lateral mixing of solids in fluidized beds – quantification of the splash-zone contribution. Powder Technol Jun. 2020;370: 96–103. https://doi.org/10.1016/J.POWTEC.2020.05.036.

[45] Kunii D, Levenspiel O. Fluidization Engineering 2nd Edition; 2013.

[46] Montgomery DC. Design and Analysis of Experiments, 10th Edition | Wiley. 2019. Accessed: Sep. 08, 2022. [Online]. Available: https://www.wiley.com/en-us/Design+and+Analysis+of+Experiments%2C+10th+Edition-p-9781119492443.